metals

MDPI

Article

Influence of Nb, Ta and Zr on the Interdiffusion Coefficients and Solid Solution Strengthening of γ-TiAl Single Phase Alloys

Lukas Haußmann [1,*], Steffen Neumeier [1,*], Johannes Bresler [1], Simon Keim [1], Florian Pyczak [2] and Mathias Göken [1]

[1] Department of Materials Science & Engineering, Institute I: General Materials Properties, Friedrich-Alexander-Universität Erlangen-Nürnberg, Martensstr. 5, 91058 Erlangen, Germany; bresler.johannes@googlemail.com (J.B.); simon.f.keim@web.de (S.K.); mathias.goeken@fau.de (M.G.)

[2] Institute of Materials Physics, Helmholtz-Zentrum Hereon, Max-Planck-Str. 1, 21502 Geesthacht, Germany; florian.pyczak@hereon.de

* Correspondence: lukas.haussmann@fau.de (L.H.); steffen.neumeier@fau.de (S.N.)

Abstract: The alloying elements Nb, Ta and Zr improve the creep properties of fully lamellar γ/α_2 titanium aluminides significantly. Since high temperature deformation mainly occurs in the γ-phase of γ/α_2 titanium aluminides, the diffusivity and the solid solution hardening effect of these three elements in the γ-phase is studied by analyzing the concentration gradients of the alloying elements and the resulting hardness across the interdiffusion zone of diffusion couples by energy dispersive X-ray diffraction and nanoindentation. The results reveal that Zr has the highest interdiffusion coefficient but also the largest solid solution hardening coefficient. The mechanical properties of single γ-phase Ti-54Al-5X alloys were investigated by strain rate jump tests. The addition of 5 at.% Nb or Ta lead to an increased strength compared to a binary γ-Ti-54Al alloy. The Zr-containing γ-TiAl alloy reveals the highest strength at 750 °C and 900 °C, which is discussed to be due to the strong solid solution hardening effect of Zr. However, in comparison to the other alloys, Ti-54Al-5Zr shows quite brittle behavior up to 900 °C. The lower diffusivity of Ta compared to Nb leads to a higher strength of the Ta-modified alloy at 900 °C.

Keywords: TiAl; γ-phase; diffusion; solid solution hardening; strain rate jump test

check for updates

Citation: Haußmann, L.; Neumeier, S.; Bresler, J.; Keim, S.; Pyczak, F.; Göken, M. Influence of Nb, Ta and Zr on the Interdiffusion Coefficients and Solid Solution Strengthening of γ-TiAl Single Phase Alloys. *Metals* **2022**, *12*, 752. https://doi.org/10.3390/met12050752

Academic Editors: Tomasz Czujko and Antonio Mateo

Received: 8 March 2022
Accepted: 16 April 2022
Published: 28 April 2022

Publisher's Note: MDPI stays neutral with regard to jurisdictional claims in published maps and institutional affiliations.

Copyright: © 2022 by the authors. Licensee MDPI, Basel, Switzerland. This article is an open access article distributed under the terms and conditions of the Creative Commons Attribution (CC BY) license (https://creativecommons.org/licenses/by/4.0/).

1. Introduction

In search of permanent improvement and optimization of existing energy conversion systems, such as aero engines or turbocharger wheels, titanium aluminides (TiAl) are an interesting alternative to the established Ni-base superalloys. Because of their good high temperature strength, oxidation and corrosion resistance in combination with their low density [1], titanium aluminides are attractive for rotatory loaded components, such as exhaust gas turbochargers [2,3]. Since these intermetallic alloys are used in a high temperature environment, their creep behavior is of major importance. The creep properties of TiAl alloys depend strongly on the microstructure. The best creep resistance is achieved by a fully lamellar microstructure with alternating α_2- and γ-laths [4,5] with small grain size and lamellar spacing [6]. Additionally, alloying elements are added to further improve the creep properties. Previous results by Bresler et al. [7] showed that the addition of 5 at.% of the element X (X = Nb, Ta or Zr) increases the creep strength of ternary Ti-44Al-5X alloys in comparison to a binary alloy with equal Al content and similar lamellar spacing, but also changes the average strain until the end of the primary creep regime is reached. While Nb slightly and Zr significantly shortens the primary creep regime, Ta leads to an increased primary creep strain. Additionally, Nb, Ta and Zr also enhance the microstructural stability by slowing down the coarsening rate and the α_2-dissolution rate during creep in the tested stress regime between 100–250 MPa at 900 °C [7]. The superior creep strength and increased microstructural stability of the ternary alloys were ascribed in previous studies [7,8] to the

solid solution hardening effect, the diffusivity, the partitioning behavior and the influence on the lattice parameters of the alloying elements Nb, Ta and Zr.

While the reduced primary creep strain in the Zr-containing alloy could be correlated with a decreased lattice misfit, the effect of the alloying elements on the creep strength could not be fully explained based on the previous work [8]. Therefore, measurements on solid solution strengthening and diffusivity of these attractive alloying elements are necessary.

In order to determine solid solution hardening and interdiffusion coefficients of the alloying elements, diffusion couples have been used quite intensively in the past for the investigation of solute diffusion in the Ni system [9,10] and Co system [11,12] as well as for investigating the diffusion in other material systems such as Cu-Sn [13] or in intermetallic phases such as NiAl [13].

The interdiffusion coefficient can be determined by evaluating the concentration profile across the interface of the alloyed and the unalloyed half of the diffusion couple [9,14]. The interdiffusion coefficients of the alloying elements Nb and Zr in the γ-TiAl phase have been studied before by Herzig et al. [15] and Divinski et al. [16] via radiotracer measurements. However, the diffusivity of Ta in the γ-phase has not been investigated so far, although it is a well-known alloying element in titanium aluminides [17,18]. Moreover, the positive effects of Nb on the mechanical properties at high temperatures are well documented in the literature [19,20], however, neither the solid solution strengthening coefficients for Ta and Zr nor for Nb have been investigated so far.

To investigate the diffusion properties of Ta in the γ-phase compared to Nb and Zr and to analyze the strengthening potential of the three decisive alloying elements Nb, Ta and Zr in γ-TiAl alloys, the solid solution hardening coefficients and interdiffusion coefficients of Nb, Ta and Zr in the γ-phase were determined in this study with diffusion couples. Durst et al. [10,21] could show that with nanoindentation on the diffusion couples the solid solution hardening coefficient of the alloying element can be determined. Additionally, strain rate jump tests were performed on single γ-phase Ti-54Al-5X alloys to correlate the influence of the alloying elements with the mechanical properties of the γ-phase as a function of the applied strain rate and temperatures. These results are essential to understand the influence of the alloying elements in γ/α_2 titanium aluminides.

2. Materials and Methods

A binary Ti-54Al alloy and three ternary Ti-54Al-5X alloys (X = Nb, Ta, Zr) were processed via vacuum arc melting from technically pure metals at the Helmholtz-Zentrum Hereon in Geesthacht. The melted buttons had a diameter of around 30 mm and a height of 15 mm. The nominal and measured compositions are given in Table 1. The concentration of the main alloying elements was determined by X-ray fluorescence analysis, the gaseous impurities by inert gas fusion and other impurities by inductively coupled plasma mass spectrometry by GfE Metalle und Materialien GmbH, Nürnberg. Elements with a concentration less than 0.01 at.% are not shown in Table 1.

Table 1. Nominal composition of Ti-54Al-5X in at.% and measured concentration in brackets below.

Alloys	Ti	Al	Nb	Ta	Zr	Cu	Fe	C	N	O
Ti-54Al	46 (45.92)	54 (53.93)	-	-	-	-	-	- (0.012)	- (0.013)	- (0.110)
Ti-54Al-5Nb	41 (40.95)	54 (53.86)	5 (5.02)	-	-	- (0.012)	-	- (0.013)	- (0.017)	- (0.114)
Ti-54Al-5Ta	41 (41.01)	54 (53.81)	-	5 (5.04)	-	-	-	- (0.029)	- (0.019)	- (0.084)
Ti-54Al-5Zr	41 (40.86)	54 (53.89)	-	-	5 (5.02)	-	- (0.075)	- (0.013)	- (0.017)	- (0.111)

The Ti-54Al-5X alloys were heat treated and homogenized at 1380 °C for different durations between 1 h and 4 h. The grain size development was determined in order to

adjust an equivalent grain size of 350 µm for all samples. The evaluation of the grain size was carried out via the line intersection method of the grain boundaries with lines in vertical and horizontal direction using the software ImageJ. The grid size was chosen to be in the order of magnitude of the average grain size. Microstructural analysis and energy dispersive X-ray spectroscopy (EDX) was performed using a ZEISS Cross Beam 1540 ESB Focused Ion Beam scanning electron microscope (SEM) with a back-scattered electron detector (BSD) from K. E. Developments Ltd. and an INCA PentaFETx3 detector (EDX) from Oxford Instruments. EDX measurements were conducted at 8 mm working distance, 20 kV excitation voltage, a 30 µm aperture and 100 ms dwell time. A Co standard was used for calibration to improve the accuracy of the measurements. For microstructural analysis, the specimens were mechanically ground and subsequently electropolished at 50 V and −30 °C for 5–10 s with Struers electrolyte A2-I.

Diffusion couples were prepared from a ternary Ti-54Al-5X cylinder and a binary Ti-54Al cylinder with 4 mm in diameter and 4 mm in height. The contact surfaces of the two samples were also mechanically ground and electropolished. Afterwards, they were mounted and fixed in a molybdenum holder with molybdenum screws and aluminium oxide shims. The diffusion couples were heat treated for 100 h at 1300 °C and 200 h at 1250 °C in a vacuum furnace and for 500 h at 1200 °C either in a quartz tube filled with argon atmosphere or a vacuum furnace depending on the oxidation sensitivity of the ternary alloy. The concentration profiles were measured via EDX and the interdiffusion coefficients were calculated according to the Sauer-Freise method [22]. This method evaluates the slope of the concentration profile to determine the interdiffusion coefficient. Due to the limitations of the method, the beginning (<1 at.%.) and the end of the concentration profiles (>4 at.%.) were not considered, as the slope of the curve here is strongly changing and the scatter of the data points reduces the accuracy of the method. To eliminate measurement-related errors, the concentration profiles were fitted with a dose-response function using a Levenberg-Marquardt algorithm [23].

Nanoindentations across the interdiffusion zone (IDZ) were conducted with a Nanoindenter XP of MTS Nanoinstruments using a Berkovich tip and the continuous stiffness method with 40 Hz. The evaluation of the hardness was done by the Oliver-Pharr method [24]. The indentation field consisted of three rows with 50 indents per row. A Poisson ratio of 0.23 for the γ-phase was assumed. To evaluate the solid solution hardening coefficient from the interdiffusion zones, the concentration and the corresponding hardness were plotted according to the Labusch-model with a solid solution strengthening exponent of 2/3 [25]. Furthermore, nanoindentations have been performed on the four bulk alloys, to calculate the bulk solid solution hardening coefficient.

Strain rate jump tests were performed in compression mode on an Instron 4505 testing machine modernized by Hegewald and Peschke using cylindrical specimens in air at room temperature, 750 °C and 900 °C. For the specimens, cylinders with a diameter of 4.2 mm were wire eroded, heat-treated, turned to 4 mm and subsequently cut and ground to a height of 6 mm. The strain rate was varied between 10^{-3} s^{-1}, 10^{-4} s^{-1} and 10^{-5} s^{-1}. The strain rate sensitivity was determined at the first and fourth strain rate jump by using Equation (2). This formula describes the strain rate sensitivity m as function of stress σ during the change of the strain rate $\dot{\varepsilon}$ [26].

$$m = \frac{\delta \, ln\sigma}{\delta \, ln\dot{\varepsilon}} \tag{1}$$

Further information on the evaluation of the strain rate sensitivity can be found in [26,27].

3. Data Evaluation

Figure 1 shows exemplarily the Nb-containing diffusion couple (Ti-54Al/Ti-54Al-5Nb) aged at 1200 °C for 500 h with the field of indents across the interface. Some Kirkendall pores are present at the interface. On the Ti-54Al side, vacancies are generated through

the faster diffusing elements which coagulate to Kirkendall pores [28]. These pores should have no influence on the analysis of the interdiffusion zone and do not seem to affect the determination of the interdiffusion coefficient.

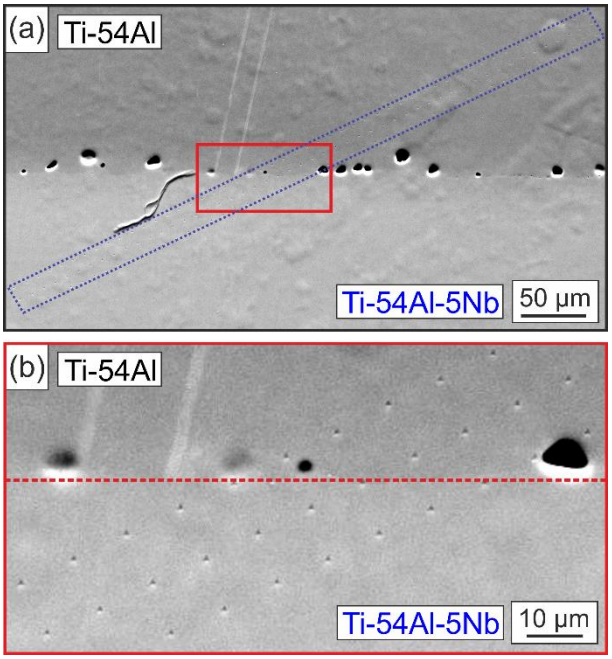


Figure 1. (**a**) Indentation field (blue) across the interface of the Nb-containing diffusion couple between Ti-54Al and Ti-54Al-5Nb aged at 1200 °C for 500 h. The area marked with a red rectangle is shown in (**b**) at a higher magnification with the interface indicated by the dashed line.

The EDX measurements along the Nb-containing diffusion couple, which were made next to the indents, are displayed in Figure 2a. All three Nb-concentration profiles show the expected S-shape. The Nb content increases from 0 at.% on the binary side to approximately 5.5 at.% on the Nb-containing, ternary side. On the ternary side of the diffusion couple, the Nb-content is slightly larger compared with the nominal Nb-content which could be due to casting segregations, which are still present after the solidification and homogenization heat treatment of the alloys [29] or due to measurement-related errors of the EDX measurement. However, as the latter should not change significantly at the different measurement sites, the effect on the interdiffusion coefficients should be negligible. The resulting interdiffusion coefficients of Nb at the different temperatures as a function of the Nb-content are plotted in Figure 2b.

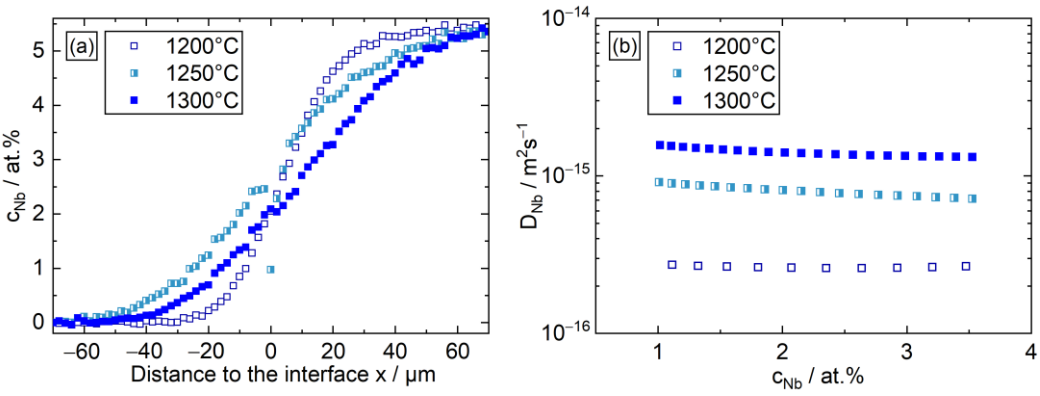


Figure 2. (**a**) Concentration C_{Nb} of Nb across the indentation zone after annealing at 1200 °C, 1250 °C and 1300 °C and (**b**) interdiffusion coefficient D_{Nb} as a function of the Nb concentration C_{Nb} at three different temperatures.

A great advantage of the diffusion couple approach is that with the same samples, diffusion and solid solution hardening coefficient can be determined. In Figure 3a, the hardness and the fitted Nb-concentration are plotted across the interface of the Nb-containing diffusion couple aged at 1200 °C for 500 h. It is clearly visible that with an increasing alloying content, the hardness increases as well. This is in good agreement with the literature on the effect of Nb on the γ-phase [30,31]. Figure 3b shows the hardness as a function of the Nb-content in the interdiffusion zone according to the Labusch model. According to Equation (1) the slope of the line in Figure 3b corresponds to the solid solution hardening coefficient K_i with the exponent a being 2/3 after the Labusch model [21]. ΔH is the hardness difference between the alloyed and the unalloyed γ-TiAl phase and c_i the concentration of the alloying element.

$$\Delta H = H_{alloyed} - H_{unalloyed} = K_i \cdot {c_i}^a \quad (2)$$

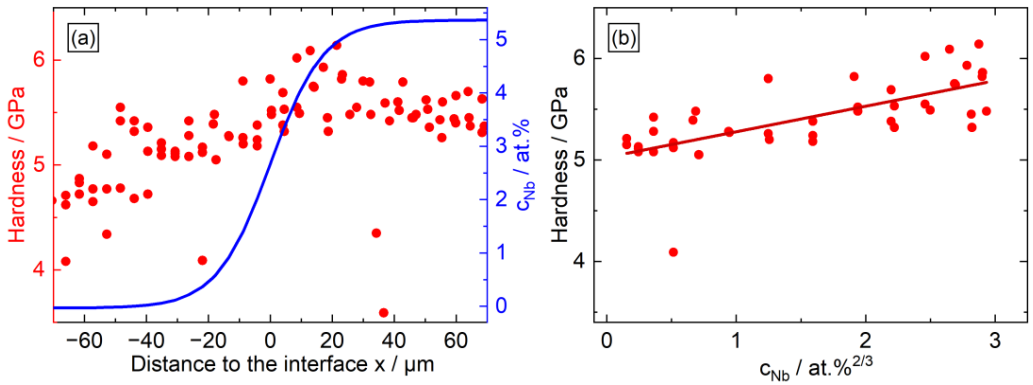


Figure 3. (**a**) Correlation between the hardness determined by nanoindentation and the fitted Nb-concentration across the Ti-54Al/Ti-54Al-5Nb diffusion couple after aging at 1200 °C for 500 h and (**b**) the hardness plotted against the Nb-concentration according to the Labusch model (reproduced from Ref. [25]) to determine the solid solution hardening coefficient.

The solid solution hardening coefficient was also calculated from nanoindentations on the bulk alloys using Equation (2) to compare it to the incremental measurements on the diffusion couples.

The analysis of the other diffusion couples showed similar microstructures with oxide free interfaces between the two alloys and similar concentration profiles. Therefore, only the results of the investigations are shown and discussed in the following chapter. The data evaluation of the other two ternary alloys Ti-54Al-5Ta and Ti-54Al-5Zr is exemplarily shown in the Supplementary Material in the Figures S1–S6.

4. Results

4.1. Interdiffusion Coefficients

The determined average interdiffusion coefficients of Nb, Ta and Zr in Ti-54Al are listed in Table 2.

Table 2. Average interdiffusion coefficient of Nb $\overline{D}_{Nb}$, Ta $\overline{D}_{Ta}$ and Zr $\overline{D}_{Zr}$ in γ-Ti-54Al.

Temperature	$\overline{D}_{Nb}$/m^2·s^{-1}	$\overline{D}_{Ta}$/m^2·s^{-1}	$\overline{D}_{Zr}$/m^2·s^{-1}
1200 °C	2.66×10^{-16}	1.88×10^{-16}	2.06×10^{-15}
1250 °C	8.18×10^{-16}	3.33×10^{-16}	6.45×10^{-15}
1300 °C	1.38×10^{-15}	7.69×10^{-16}	1.08×10^{-14}

The activation energy for interdiffusion has been determined from an Arrhenius diagram (Figure 4) and the results are compared with literature data [15]. Using Equation (3),

the frequency factor D_0 ($m^2 \cdot s^{-1}$) and the activation energy Q ($kJ \cdot mol^{-1}$) can be calculated with the universal gas constant R ($J \cdot mol^{-1} \cdot K^{-1}$) and the temperature T (°C) (see Table 3).

$$D = D_0 \cdot \exp\left(-\frac{Q}{RT}\right) \quad (3)$$

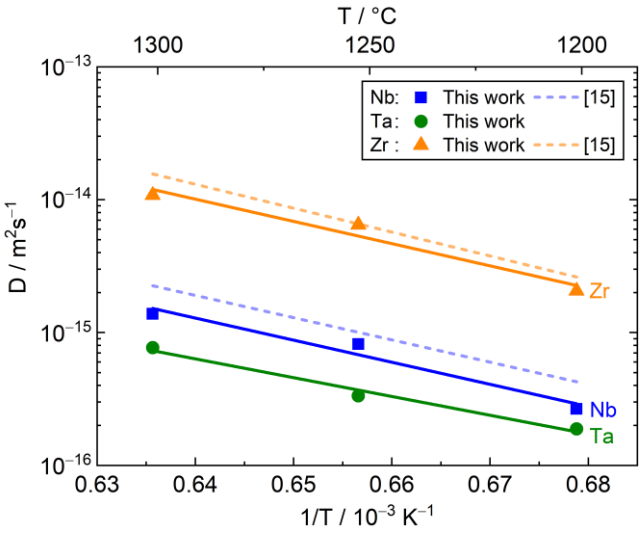


Figure 4. Arrhenius-plot of the average interdiffusion coefficients D of Nb, Ta and Zr determined in this work, compared with literature data from Herzig et al. (reproduced from Ref. [15]), in a temperature range of 1200–1300 °C.

Table 3. Activation energy Q and frequency factor D_0 of the alloying elements Niobium, Tantalum and Zirconium in γ-Ti-54Al.

Element	Activation Energy Q/kJ·mol^{-1}	Frequency Factor/m^2·s^{-1}
Nb	318	5.63×10^{-5}
Ta	271	7.12×10^{-7}
Zr	320	5.19×10^{-4}

The interdiffusion coefficients of Nb and Zr determined in this work are in good accordance with the ones from literature [15,16]. The slight difference could originate from the different methods which were used to obtain the interdiffusion coefficient. Herzig et al. [15] as well as Divinski et al. [16] applied the radiotracer method, whereas in this work diffusion couples were used. Zr shows the highest diffusivity, followed by Nb and Ta. For Ta no literature data are available so far. However, the trend of the diffusivity of the three elements can also be found in other alloy systems like Ni [14] or Co solid solutions [11].

4.2. Solid Solution Hardening Coefficient

The solid solution hardening coefficients determined on the diffusion couples and the bulk alloys fit quite well to each other, see Table 4. As already stated in literature [32–34], the results confirm that Nb is an effective solid solution strengthener that improves the mechanical properties and creep strength in titanium aluminides. However, Ta and Zr are likewise or even more effective than Nb. Since the solid solution hardening coefficients determined from the diffusion couples are based on a multitude of data points, we assume these coefficients to be more precise. The slightly higher strengthening coefficient of Ta compared to Nb would also fit the assumption that Ta is a slightly more efficient solid solution hardener than Nb, as proposed by Vojtěch et al. [18]. In any case, Zr has the highest solid solution hardening potential that is about 1.8 times larger than that of Nb and still 1.6 times larger than that of Ta.

Table 4. Average values of the solid solution hardening coefficients K_{ssh} (IDZ) of Nb, Ta and Zr determined on the diffusion couples as well as Hardness H (Bulk) and solid solution hardening coefficients K_{ssh} (Bulk) for all investigated alloys measured on the bulk materials.

Alloy	Kssh (IDZ)/GPa/(at.%$^{2/3}$)	H (Bulk)/GPa	Kssh (Bulk)/GPa/(at.%$^{2/3}$)
Ti-54Al	-	3.46 ± 0.38	-
Ti-54Al-5Nb	0.26	4.38 ± 0.41	0.31 ± 0.38
Ti-54Al-5Ta	0.30	4.22 ± 0.49	0.26 ± 0.42
Ti-54Al-5Zr	0.47	4.99 ± 0.41	0.52 ± 0.38

4.3. Strain Rate Jump Tests

For the evaluation of the mechanical properties of the pure γ-phase Ti-54Al-5X alloys, strain rate jump tests at room temperature and elevated temperatures were performed in compression at room temperature. The stress strain curves of the four alloys at room temperature are shown in Figure 5. At this testing temperature all investigated alloys showed brittle failure. While Ti-54Al, Ti-54Al-5Nb and Ti-54Al-5Ta exhibit failure strains between 13% and 17%, the brittle behavior is significantly more pronounced for the Ti-54Al-5Zr alloy, which fails at only 3% strain. This coincides with results from Kawabata et al. [35], who observed a significantly reduced fracture strain with increasing Zr additions. This reduced fracture strain of Ti-54Al-5Zr also leads to a strongly decreased strength. The stress strain curves of Ti-54Al-5Nb and Ti-54Al-5Ta at room temperature show no overall beneficial effect of Nb or Ta additions compared to Ti-54Al.

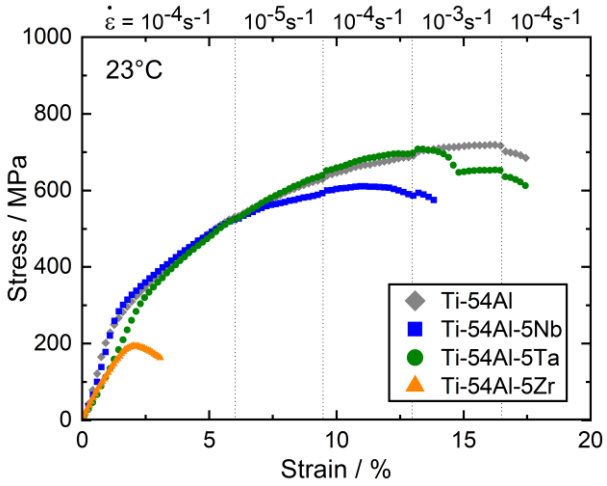


Figure 5. Compression stress-strain curves of strain rate jump tests at room temperature of the Ti-54Al-5X alloys and Ti-54Al.

At higher temperatures of 750 °C and 900 °C all alloying elements lead to an increase in strength of the γ-phase alloys as shown in Figure 6. This confirms the known beneficial effect of Nb on the mechanical properties of the γ-phase, which was shown by Schuster et al. [30]. The strength increase is clearly the highest in the case of Zr addition, which leads to a strength 1.5 to 2.6 times higher than the other ternary alloys. However, Ti-54Al-5Zr still shows significant brittle behavior at 750 °C, with a failure at 11% plastic deformation. Furthermore, despite the relatively smooth stress strain curves, SEM investigations on the tested samples revealed that Ti-54Al tested at 750 °C and Ti-54Al-5Zr tested at 900 °C still fail somewhat brittle due to internal crack formation.

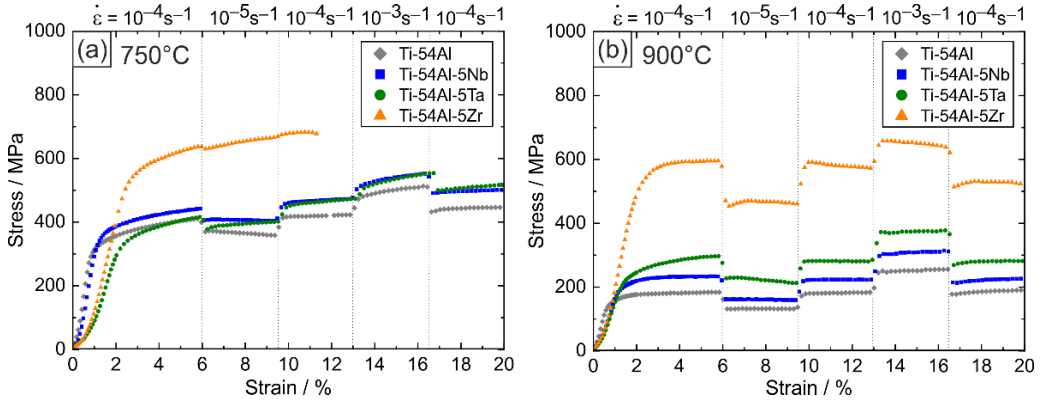


Figure 6. Compressional stress-strain curves of strain rate jump tests at (**a**) 750 °C and (**b**) 900 °C of the Ti-54Al-5X alloys and Ti-54Al.

Comparing Ti-54Al-5Nb and Ti-54Al-5Ta, at 750 °C Nb and Ta additions lead to a similar and slightly improved strength, whereas at 900 °C Ti-54Al-5Ta exhibits an approximately 60 MPa higher strength than Ti-54Al-5Nb. Figure 7 shows the strain rate sensitivity and the 0.2% compressive strength of the Ti-54Al-5X alloys at 750 °C and 900 °C.

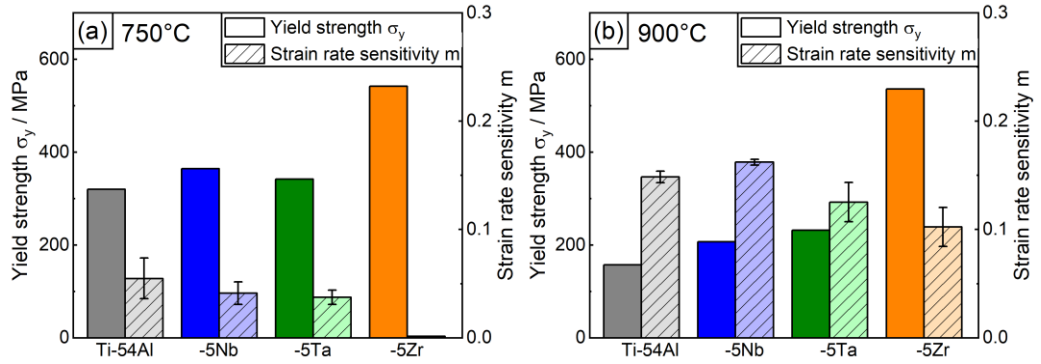


Figure 7. Strain rate sensitivity m and 0.2% compressive strength $\sigma_{p0.2}$ of the Ti-54Al-5X alloys and Ti-54Al at (**a**) 750 °C and (**b**) 900 °C.

It can be seen that the 0.2% compressive strengths of Ti-54Al, Ti-54Al-5Nb and Ti-54Al-5Ta decrease significantly by around 100 to 150 MPa with the temperature increase, whereas the 0.2% compressive strength of Ti-54Al-5Zr stays nearly constant. It is also evident that with increasing temperature the strain rate sensitivity increases for all alloys, which indicates an increasing influence of thermally activated processes during deformation. Unexpectedly, the Ti-54Al-5Zr alloy shows at both temperatures the lowest strain rate sensitivity, although the interdiffusion coefficient of Zr is clearly the highest, compared to Nb and Ta.

5. Discussion

The results show that the interdiffusion as well as the strengthening coefficients of the alloying elements correlate to a certain extent with the Goldschmidt radii [36,37] of the elements and the atomic size mismatch between the solute and the host Ti lattice atoms (see Figure 8). The diffusivity of the alloying elements is mainly determined by the bonding between the solute atom and the host atoms. Janotti et al. [37] showed that with increasing Goldschmidt radius the interdiffusion coefficient increases in Ni solid solutions [14,38]. They argue that larger transition metal atoms form weaker bonds to their next neighbors and therefore diffuse faster. Apparently, the higher diffusivity of Zr in γ-TiAl also seems to be somehow linked with its larger atomic radius.

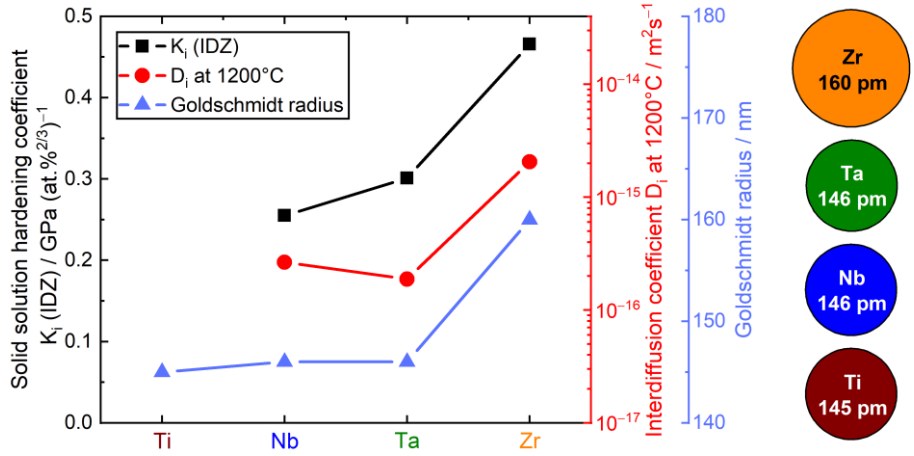


Figure 8. Solid solution hardening coefficients K_i, interdiffusion coefficients D_i determined on the interdiffusion zones and the Goldschmidt radii (reproduced from Ref. [36]) of the three investigated alloying elements Nb, Ta and Zr and Ti in γ-Ti-54Al.

Solid solution hardening at low temperatures is closely related to the size difference between the solute and surrounding host atoms. Ti has a Goldschmidt radius of 145 pm while Nb and Ta with 146 pm have slightly lager radii, which explains the moderate and similar strengthening effect of both elements. The slight difference in the solid solution hardening coefficient between Nb and Ta could be explained by slightly different bonding strengths of these two elements or measurement-related uncertainties. The significantly larger solid solution hardening coefficient of Zr could be due to the much larger Goldschmidt radius. The lattice distortion induced by the 10% larger radius seems to be of considerable influence. At higher temperatures, solid solution hardening is also influenced by the diffusivity. It seems that the influence of thermally activated processes at 750 °C ($T/T_m \approx 0.6$) is still small and that the solutes can be regarded as rigid obstacles for the moving dislocations in the strain rate regime investigated here. At 900 °C ($T/T_m \approx 0.7$) the influence of the diffusivity of Nb and Ta becomes more noticeable. Ta has a lower interdiffusion coefficient than Nb, hence the deformation resistance of the Ti-54Al-5Ta alloy is higher at 900 °C in contrast to the Ti-54Al-5Nb alloy (see Figure 6b). This is also in good accordance with Vojtěch et al. [18] and Saage et al. [39], who assumed that the superior creep properties of a Ta-containing alloy compared to an Nb-containing titanium aluminide alloy results from the lower diffusivity of Ta. This work also confirms the previously made assumption on the creep experiments of fully lamellar Ti-44Al-5X alloys [7]. The excellent creep properties of the Ti-44Al-5Ta and Ti-44Al-5Zr alloys at 900 °C were ascribed to the low diffusivity of the alloying element Ta and the strong solid solution hardening effect of Zr due to the large atomic size mismatch. Nevertheless, since Zr exhibits a nearly 10 times higher interdiffusion coefficient than Nb and Ta, the strength at high temperatures and low strain rates should be much smaller. Since Zr decreases even stronger than Nb and Ta, the c/a-ratio of the γ-phase of fully lamellar titanium aluminides [8,40], and an easier plastic deformation and thus lower strength could be expected.

The significantly higher strength could be a result of the formation of small precipitates of a second phase or a higher solubility for small atoms such as oxygen or hydrogen and therefore an additional solid solution hardening effect due to the Zr addition. However, neither the microstructural nor the chemical analysis showed the presence of a second phase or significant differences in the chemical composition of the alloys (see Table 1). It rather seems that Zr influences the deformation mechanisms or atomic bonding character in the ordered $L1_0$-γ-phase in a way that could explain the observed findings. This is supported by the more brittle behavior of Ti-54Al-5Zr as the fractographic investigations on the tested samples showed. Pronounced cracking was observed at room temperature for all alloys. However, Ti-54Al-5Zr is the only alloy which still shows visible crack formation

at a testing temperature of up to 900 °C. Due to the layer wise crystal structure of the γ-phase, the deformation mechanisms and dislocation interactions are quite complex. Due to splitting and cross slipping, the dislocations can form sessile configurations [41–45]. Furthermore, there is a strong bidirectional bonding within the layers of Ti-atoms in the $L1_0$-structure, which leads to an anisotropy in the Peierls stress. This can cause dislocations to be sessile or to have a reduced mobility [41,43,46], which lead to a distinct flow stress anomaly and a low ductility [43–45]. Tanda et al. [40] have investigated the influence of different Zr additions to γ-TiAl and they could observe a much more pronounced yield stress anomaly with a significantly higher peak stress compared to binary alloys and no considerable plasticity could be measured in alloys with Zr additions over 5 at.% below 800 °C. They also investigated the lattice parameter changes with increasing Zr content and noticed that the changes are not monotonic and not similar for the a- and c-direction but the c/a-ratio is generally decreased with increasing Zr-content [40]. This was also found in a previous study by the authors of this work [8]. This is attributed to a modification of the covalent nature of the bonding between the constituent elements. The alteration of the bonding type could also explain the reduced ductility as well as the improved mechanical properties of Ti-54Al-5Zr despite the decreased c/a-ratio, which generally should increase the ductility. A change to a more covalent bonding character could increase the local Peierls stresses and the peak stress of the yield stress anomaly with a reduction in ductility. However, more detailed investigations on the influences of the alloying additions Nb, Ta and Zr on the deformation mechanisms in γ-TiAl have to be carried out to confirm this.

6. Conclusions

A detailed analysis about the influence of the alloying elements Nb, Ta and Zr on the diffusivity and solid solution hardening in the γ-TiAl phase has been performed, from which the following conclusions can be drawn:

- Ta is the slowest diffusing element, followed by Nb and Zr in γ-Ti-54Al single phase alloys.
- The solid solution hardening coefficients determined on diffusion couples are 0.26 GPa/(at.%$^{2/3}$) for Nb, 0.30 GPa/(at.%$^{2/3}$) for Ta and 0.47 GPa/(at.%$^{2/3}$) for Zr in the γ-TiAl phase, which correlates with the atomic size mismatch between the solutes and Ti. The solid solution hardening coefficients determined on the bulk alloys also show a higher solid solution hardening coefficient of Zr than Nb and Ta and are therefore in good agreement with the measurements on the diffusion couples.
- The addition of 5 at.% Nb or Ta increases the strength compared to a binary γ-Ti54Al alloy. The Zr-containing γ-TiAl single phase alloy reveals the highest strength at 750 °C and 900 °C due to the strong solid solution hardening effect of Zr, but shows in comparison to the other alloys a quite brittle behavior up to 900 °C. The lower diffusivity of Ta compared to Nb leads to a higher strength of the Ta-modified alloy at 900 °C.

Supplementary Materials: The following are available online at https://www.mdpi.com/article/10.3390/met12050752/s1, Figure S1: Indentation field (green) across the interface of the Ta-containing diffusion couple of Ti-54Al and Ti-54Al-5Ta aged at 1300 °C for 100 h, Figure S2: (a) Concentration c_{Ta} of Ta across the indentation zone after annealing at 1200 °C, 1250 °C and 1300 °C and (b) interdiffusion coefficient D_{Ta} as a function of the Ta concentration c_{Ta} at three different temperatures, Figure S3: (a) Correlation between the hardness determined by nanoindentation and the fitted Ta-concentration across the Ti-54Al/Ti-54Al-5Ta diffusion couple after aging at 1300 °C for 100 h and (b) the hardness plotted against the Ta-concentration according to the Labusch model [47] to determine the solid solution hardening coefficient, Figure S4: Indentation field (orange) across the interface of the Zr-containing diffusion couple of Ti-54Al and Ti-54Al-5Zr aged at 1200 °C for 500 h, Figure S5: (a) Concentration c_{Zr} of Zr across the indentation zone after annealing at 1200 °C, 1250 °C and 1300 °C and (b) interdiffusion coefficient D_{Zr} as a function of the Zr concentration c_{Zr} at three different temperatures, Figure S6: (a) Correlation between the hardness determined by nanoindentation and the fitted Zr-concentration across the Ti-54Al/Ti-54Al-5Zr diffusion couple after

aging at 1200 °C for 500 h and (b) the hardness plotted against the Ta-concentration according to the Labusch model [47] to determine the solid solution hardening coefficient.

Author Contributions: Conceptualization, S.N., J.B., F.P. and M.G.; methodology, S.N., J.B., S.K. and F.P.; formal analysis, L.H., J.B. and S.K.; investigation, L.H., J.B. and S.K.; resources, M.G.; writing—original draft preparation, J.B. and L.H.; writing—review and editing, L.H., S.N., F.P. and M.G.; visualization, L.H.; supervision, S.N. and M.G.; project administration, M.G.; funding acquisition, M.G. All authors have read and agreed to the published version of the manuscript.

Funding: The authors acknowledge financially support by the Deutsche Forschungsgemeinschaft (DFG) within the framework of the DFG graduate school 1229.

Data Availability Statement: The research data are available from the corresponding author on reasonable request.

Acknowledgments: The authors would like to acknowledge Jonathan D.H. Paul and Markus Rackel for processing the four different alloys and Volker Güther from the GfE Metalle und Materialien GmbH of the Advanced Metallurgical Group N.V. for the chemical analysis of the four alloys.

Conflicts of Interest: The authors declare no conflict of interest.

References

1. Chen, Y.Y.; Yang, F.; Kong, F.T.; Xiao, S.L. Microstructure, Mechanical Properties, Hot Deformation and Oxidation Behavior of Ti–45Al–5.4V–3.6Nb–0.3Y Alloy. *J. Alloys Compd.* **2010**, *498*, 95–101. [CrossRef]
2. Noda, T. Application of Cast Gamma TiAl for Automobiles. *Intermetallics* **1998**, *6*, 709–713. [CrossRef]
3. Tetsui, T.; Ono, S. Endurance and Composition and Microstructure Effects on Endurance of TiAl Used in Turbochargers. *Intermetallics* **1999**, *7*, 689–697. [CrossRef]
4. Worth, B.D.; Jones, J.W.; Allison, J.E. Creep Deformation in Near-γ TiAl: The Influence of Microstructure on Creep Deformation in Ti-49Al-1V. *Metall. Mater. Trans. A* **1995**, *26*, 2947–2959. [CrossRef]
5. Maruyama, K.; Yamamoto, R.; Nakakuki, H.; Fujitsuna, N. Effects of Lamellar Spacing, Volume Fraction and Grain Size on Creep Strength of Fully Lamellar TiAl Alloys. *Mater. Sci. Eng. A* **1997**, *239*, 419–428. [CrossRef]
6. Cao, G.; Fu, L.; Lin, J.; Zhang, Y.; Chen, C. The Relationships of Microstructure and Properties of a Fully Lamellar TiAl Alloy. *Intermetallics* **2000**, *8*, 647–653. [CrossRef]
7. Bresler, J.; Neumeier, S.; Ziener, M.; Pyczak, F.; Göken, M. The Influence of Niobium, Tantalum and Zirconium on the Microstructure and Creep Strength of Fully Lamellar γ/α_2 Titanium Aluminides. *Mater. Sci. Eng. A* **2019**, *744*, 46–53. [CrossRef]
8. Neumeier, S.; Bresler, J.; Zenk, C.; Haußmann, L.; Stark, A.; Pyczak, F.; Göken, M. Partitioning Behavior of Nb, Ta, and Zr in Fully Lamellar γ/α_2 Titanium Aluminides and Its Effect on the Lattice Misfit and Creep Behavior. *Adv. Eng. Mater.* **2021**, *23*, 2100156. [CrossRef]
9. Karunaratne, M.S.A.; Carter, P.; Reed, R.C. Interdiffusion in the Face-Centred Cubic Phase of the Ni–Re, Ni–Ta and Ni–W Systems between 900 and 1300 °C. *Mater. Sci. Eng. A* **2000**, *281*, 229–233. [CrossRef]
10. Franke, O.; Durst, K.; Göken, M. Nanoindentation Investigations to Study Solution Hardening in Ni-Based Diffusion Couples. *J. Mater. Res.* **2011**, *24*, 1127–1134. [CrossRef]
11. Neumeier, S.; Rehman, H.U.; Neuner, J.; Zenk, C.H.; Michel, S.; Schuwalow, S.; Rogal, J.; Drautz, R.; Göken, M. Diffusion of Solutes in Fcc Cobalt Investigated by Diffusion Couples and First Principles Kinetic Monte Carlo. *Acta Mater.* **2016**, *106*, 304–312. [CrossRef]
12. Ustad, T.; Sørum, H. Interdiffusion in the Fe-Ni, Ni-Co, and Fe-Co Systems. *Phys. Status Solidi (a)* **1973**, *20*, 285–294. [CrossRef]
13. Gong, X.; Ma, Y.; Guo, H.; Gong, S. Effect of Thermal Cycling on Microstructure Evolution and Elements Diffusion Behavior near the Interface of Ni/NiAl Diffusion Couple. *J. Alloys Compd.* **2015**, *642*, 117–123. [CrossRef]
14. Fu, C.L.; Reed, R.C.; Janotti, A.; Krcmar, M. On the Diffusion of Alloying Elements in the Nickel-Base Superalloys. *Superalloys* **2004**, *2004*, 867–876.
15. Herzig, C.; Przeorski, T.; Friesel, M.; Hisker, F.; Divinski, S. Tracer Solute Diffusion of Nb, Zr, Cr, Fe, and Ni in γ-TiAl: Effect of Preferential Site Occupation. *Intermetallics* **2001**, *9*, 461–472. [CrossRef]
16. Divinski, S.; Hisker, F.; Klinkenberg, C.; Herzig, C. Niobium and Titanium Diffusion in the High Niobium-Containing Ti–54Al–10Nb Alloy. *Intermetallics* **2006**, *14*, 792–799. [CrossRef]
17. Loretto, M.H.; Wu, Z.; Chu, M.Q.; Saage, H.; Hu, D.; Attallah, M.M. Deformation of Microstructurally Refined Cast Ti46Al8Nb and Ti46Al8Ta. *Intermetallics* **2012**, *23*, 1–11. [CrossRef]
18. Vojtěch, D.; Popela, T.; Hamáček, J.; Kützendörfer, J. The Influence of Tantalum on the High Temperature Characteristics of Lamellar Gamma+alpha 2 Titanium Aluminide. *Mater. Sci. Eng. A* **2011**, *528*, 8557–8564. [CrossRef]
19. Liu, Z.C.; Lin, J.P.; Li, S.J.; Chen, G.L. Effects of Nb and Al on the Microstructures and Mechanical Properties of High Nb Containing TiAl Base Alloys. *Intermetallics* **2002**, *10*, 653–659. [CrossRef]

20. Zhang, W.; Liu, Z.; Chen, G.; Kim, Y.-W. Deformation Mechanisms in a High-Nb Containing γ–TiAl Alloy at 900 °C. *Mater. Sci. Eng. A* **1999**, *271*, 416–423. [CrossRef]
21. Durst, K.; Franke, O.; Böhner, A.; Göken, M. Indentation Size Effect in Ni–Fe Solid Solutions. *Acta Mater.* **2007**, *55*, 6825–6833. [CrossRef]
22. Sauer, F.; Freise, V. Diffusion in Binären Gemischen Mit Volumenänderung. *Z. Elektrochem. Ber. Bunsenges. Phys. Chem.* **1962**, *66*, 353–362. [CrossRef]
23. Moré, J.J. The Levenberg-Marquardt Alorithm: Implementation and Theory. In *Numerical Analysis*; Springer: Berlin/Heidelberg, Germany, 1978; pp. 105–116.
24. Oliver, W.C.; Pharr, G.M. An Improved Technique for Determining Hardness and Elastic Modulus Using Load and Displacement Sensing Indentation Experiments. *J. Mater. Res.* **1992**, *7*, 1564–1583. [CrossRef]
25. Labusch, R. Statistische Theorien der Mischkristallhärtung. *Acta Metall.* **1972**, *20*, 917–927. [CrossRef]
26. Hart, E.W. Theory of the Tensile Test. *Acta Metall.* **1967**, *15*, 351–355. [CrossRef]
27. Ghosh, A.K. On the Measurement of Strain-Rate Sensitivity for Deformation Mechanism in Conventional and Ultra-Fine Grain Alloys. *Mater. Sci. Eng. A* **2007**, *463*, 36–40. [CrossRef]
28. Smigelskas, A.D.; Kirkendall, E.O. Zinc Diffusion in Alpha Brass. *Trans. AIME* **1946**, *171*, 130–142.
29. Schuster, J.C.; Palm, M. Reassessment of the Binary Aluminum-Titanium Phase Diagram. *J. Phase Equilibria Diffus.* **2006**, *27*, 255–277. [CrossRef]
30. Tetsui, T. Effects of High Niobium Addition on the Mechanical Properties and High-Temperature Deformability of Gamma TiAl Alloy. *Intermetallics* **2002**, *10*, 239–245. [CrossRef]
31. Gebhard, S.; Pyczak, F.; Göken, M. Microstructural and Micromechanical Characterisation of TiAl Alloys Using Atomic Force Microscopy and Nanoindentation. *Mater. Sci. Eng. A* **2009**, *523*, 235–241. [CrossRef]
32. Schwaighofer, E.; Rashkova, B.; Clemens, H.; Stark, A.; Mayer, S. Effect of Carbon Addition on Solidification Behavior, Phase Evolution and Creep Properties of an Intermetallic b-Stabilized g-TiAl Based Alloy. *Intermetallics* **2014**, *46*, 173–184. [CrossRef]
33. Sun, F.-S.; Cao, C.-X.; Yan, M.-G.; Kim, S.-E. Alloying Mechanism of Beta Stabilizers in a TiAl Alloy. *Metall. Mater. Trans. A* **2001**, *32*, 1573–1589. [CrossRef]
34. Zhang, W.; Deevi, S.; Chen, G. On the Origin of Superior High Strength of Ti–45Al–10Nb Alloys. *Intermetallics* **2002**, *10*, 403–406. [CrossRef]
35. Kawabata, T.; Fukai, H.; Izumi, O. Effect of Ternary Additions on Mechanical Properties of TiAl. *Acta Mater.* **1998**, *46*, 2185–2194. [CrossRef]
36. Goldschmidt, V.M. Crystal Structure and Chemical Constitution. *Trans. Faraday Soc.* **1929**, *25*, 253–283. [CrossRef]
37. Janotti, A.; Krcmar, M.; Fu, C.L.; Reed, R.C. Solute Diffusion in Metals: Larger Atoms Can Move Faster. *Phys. Rev. Lett.* **2004**, *92*, 085901. [CrossRef]
38. Karunaratne, M.S.A.; Reed, R.C. Interdiffusion of Niobium and Molybdenum in Nickel between 900–1300 °C. In Proceedings of the Diffusion in Materials—DIMAT2004, Cracow, Poland, 18–23 July 2004; Volume 237, pp. 420–425.
39. Saage, H.; Huang, A.J.; Hu, D.; Loretto, M.H.; Wu, X. Microstructures and Tensile Properties of Massively Transformed and Aged Ti46Al8Nb and Ti46Al8Ta Alloys. *Intermetallics* **2009**, *17*, 32–38. [CrossRef]
40. Tanda, D.; Tanabe, T.; Tamura, R.; Takeuchi, S. Synthesis of Ternary L10 Compounds of Ti–Al–Zr System and Their Mechanical Properties. *Mater. Sci. Eng. A* **2004**, *387–389*, 991–995. [CrossRef]
41. Court, S.A.; Vasudevan, V.K.; Fraser, H.L. Deformation Mechanisms in the Intermetallic Compound TiAl. *Philos. Mag. A* **1990**, *61*, 141–158. [CrossRef]
42. Sriram, S.; Dimiduk, D.M.; Hazzledine, P.M.; Vasudevan, V.K. The Geometry and Nature of Pinning Points of ½ ⟨110] Unit Dislocations in Binary TiAl Alloys. *Philos. Mag. A* **1997**, *76*, 965–993. [CrossRef]
43. Viguier, B.; Hemker, K.J.; Bonneville, J.; Louchet, F.; Martin, J.-L. Modelling the Flow Stress Anomaly in γ-TiAl I. Experimental Observations of Dislocation Mechanisms. *Philos. Mag. A* **1995**, *71*, 1295–1312. [CrossRef]
44. Greenberg, B.A.; Gornostirev, Y.N. Possible Factors Affecting the Brittleness of the Intermetallic Compound TiAl. I. Transformations of Dislocations to Non-Planar Configurations. *Scr. Metall.* **1988**, *22*, 853–857. [CrossRef]
45. Kawabata, T.; Kanai, T.; Izumi, O. Positive Temperature Dependence of the Yield Stress in TiAl L10 Type Superlattice Intermetallic Compound Single Crystals at 293–1273 K. *Acta Metall.* **1985**, *33*, 1355–1366. [CrossRef]
46. Greenberg, B.F.; Anisimov, V.I.; Gornostirev, Y.N.; Taluts, G.G. Possible Factors Affecting the Brittleness of the Intermetallic Compound TiAl. II. Peierls Manyvalley Relief. *Scr. Metall.* **1988**, *22*, 859–864. [CrossRef]
47. Labusch, R. A Statistical Theory of Solid Solution Hardening. *Phys. Status Solidi B* **1970**, *41*, 659–669. [CrossRef]